

COMPRESSION OF DEEP CONVOLUTIONAL NEURAL NETWORKS FOR FAST AND LOW POWER MOBILE APPLICATIONS

Yong-Deok Kim¹, Eunhyeok Park², Sungjoo Yoo², Taelim Choi¹, Lu Yang¹ & Dongjun Shin¹

¹Software R&D Center, Device Solutions, Samsung Electronics, South Korea
{yd.mlg.kim, tl.choi, lu2014.yang, d.j.shin}@samsung.com

²Department of Computer Science and Engineering, Seoul National University, South Korea
{canusglow, sungjoo.yoo}@gmail.com

ABSTRACT

Although the latest high-end smartphone has powerful CPU and GPU, running deeper convolutional neural networks (CNNs) for complex tasks such as *ImageNet* classification on mobile devices is challenging. To deploy deep CNNs on mobile devices, we present a simple and effective scheme to compress the entire CNN, which we call **one-shot whole network compression**. The proposed scheme consists of three steps: (1) rank selection with variational Bayesian matrix factorization, (2) Tucker decomposition on kernel tensor, and (3) fine-tuning to recover accumulated loss of accuracy, and each step can be easily implemented using publicly available tools. We demonstrate the effectiveness of the proposed scheme by testing the performance of various compressed CNNs (*AlexNet*, *VGG-S*, *GoogLeNet*, and *VGG-16*) on the smartphone. Significant reductions in model size, runtime, and energy consumption are obtained, at the cost of small loss in accuracy. In addition, we address the important implementation level issue on 1×1 convolution, which is a key operation of *inception* module of *GoogLeNet* as well as CNNs compressed by our proposed scheme.

1 INTRODUCTION

Deployment of convolutional neural networks (CNNs) for computer vision tasks on mobile devices is gaining more and more attention. On mobile applications, it is typically assumed that training is performed on the server and test or inference is executed on the mobile devices. One of the most critical issues in mobile applications of CNNs is that mobile devices have strict constraints in terms of computing power, battery, and memory capacity. Thus, it is imperative to obtain CNNs tailored to the limited resources of mobile devices.

Deep neural networks are known to be over-parameterized, which facilitates convergence to good local minima of the loss function during training (Hinton et al., 2012; Denil et al., 2013). To improve test-time performance on mobile devices, such redundancy can be removed from the trained networks without noticeable impact on accuracy. Recently, there are several studies to apply low-rank approximations to compress CNNs by exploiting redundancy (Jaderberg et al., 2014; Denton et al., 2014; Lebedev et al., 2015). Such compressions typically focus on convolution layers since they dominate total computation cost especially in deep neural networks (Simonyan & Zisserman, 2015; Szegedy et al., 2015). Existing methods, though effective in reducing the computation cost of a single convolutional layer, introduce a new challenge called whole network compression which aims at compressing the entire network.

Whole network compression: It is nontrivial to compress whole and very deep CNNs for complex tasks such as *ImageNet* classification. Recently, Zhang et al. (2015b;a) showed that entire convolutional layers can be accelerated with “asymmetric (3d)” decomposition. In addition, they also presented the effective rank selection and optimization method. Although their proposed decom-

position of layers can be easily implemented in popular development tools (e.g. Caffe, Torch, and Theano), the rank selection and optimization parts still require because they consist of multiple steps and depend on the output of previous layers. In this paper, we present much simpler but still powerful whole network compression scheme which takes entire convolutional and fully-connected layers into account.

Contribution: This paper makes the following major contributions.

- We propose a *one-shot whole network compression scheme* which consists of simple three steps: (1) rank selection, (2) low-rank tensor decomposition, and (3) fine-tuning.
- In the proposed scheme, Tucker decomposition (Tucker, 1966) with the rank determined by a global analytic solution of variational Bayesian matrix factorization (VBMF) (Nakajima et al., 2012) is applied on each kernel tensor. Note that we simply minimize the reconstruction error of linear kernel tensors instead of non-linear responses. Under the Tucker decomposition, the accumulated loss of accuracy can be sufficiently recovered by using fine-tuning with *ImageNet* training dataset.
- Each step of our scheme can be easily implemented using publicly available tools, (Nakajima, 2015) for VBMF, (Bader et al., 2015) for Tucker decomposition, and Caffe for fine-tuning.
- We evaluate various compressed CNNs (*AlexNet*, *VGG-S*, *GoogLeNet*, and *VGG-16*) on both Titan X and smartphone. Significant reduction in model size, runtime, and energy consumption are obtained, at the cost of small loss in accuracy.
- By analysing power consumption over time, we observe interesting behaviours of 1×1 convolution which is the key operation in our compressed model as well as in *inception* module of *GoogLeNet*. Although the 1×1 convolution is mathematically simple operation, it is considered to lack in cache efficiency, hence it is the root cause of gap between theoretical and practical speed up ratios.

This paper is organized as follows. Section 2 reviews related work. Section 3 explains our proposed scheme. Section 4 gives experimental results. Section 5 summarizes the paper.

2 RELATED WORK

2.1 CNN COMPRESSION

CNN usually consists of convolutional layers and fully-connected layers which dominate computation cost and memory consumption respectively. After Denil et al. (2013) showed the possibility of removing the redundancy of neural networks, several CNN compression techniques have been proposed. A recent study (Denton et al., 2014) showed that the weight matrix of a fully-connected layer can be compressed by applying truncated singular value decomposition (SVD) without significant drop in the prediction accuracy. More recently, various methods based on vector quantization (Gong et al., 2014), hashing techniques (Chen et al., 2015), circulant projection (Cheng et al., 2015), and tensor train decomposition (Novikov et al., 2015) were proposed and showed better compression capability than SVD. To speed up the convolutional layers, several methods based on low-rank decomposition of convolutional kernel tensor were proposed (Denton et al., 2014; Jaderberg et al., 2014; Lebedev et al., 2015), but they compress only single or a few layers.

Concurrent with our work, Zhang et al. (2015b) presented “asymmetric (3d) decomposition” to accelerate the entire convolutional layers, where the original $D \times D$ convolution is decomposed to $D \times 1$, $1 \times D$, and 1×1 convolution. In addition, they also present a rank selection method based on PCA accumulated energy and an optimization method which minimizes the reconstruction error of non-linear responses. In the extended version (Zhang et al., 2015a), the additional fine-tuning of entire network was considered for further improvement. Compared with these works, our proposed scheme is different in that (1) Tucker decomposition is adopted to compress the entire convolutional and fully-connected layers, (2) the kernel tensor reconstruction error is minimized instead of non-linear response, (3) a global analytic solution of VBMF (Nakajima et al., 2012) is applied to determine the rank of each layer, and (4) a single run of fine-tuning is performed to account for the accumulation of errors.

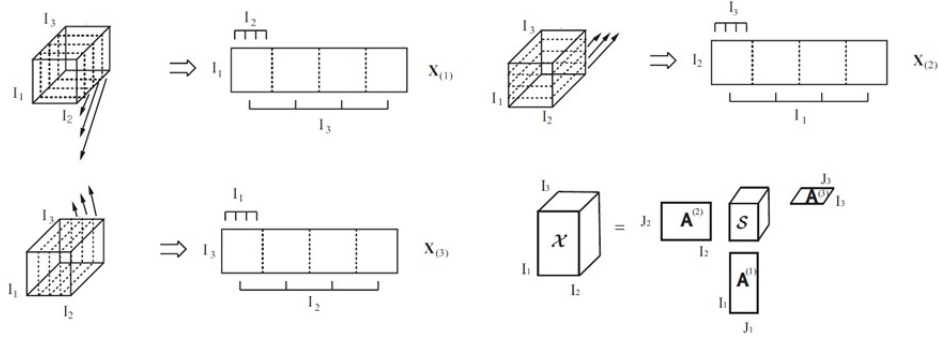


Figure 1: Mode-1 (top left), mode-2 (top right), and mode-3 (bottom left) matricization of the 3-way tensor. They are constructed by concatenation of frontal, horizontal, and vertical slices, respectively. (Bottom right): Illustration of 3-way Tucker decomposition. The original tensor \mathcal{X} of size $I_1 \times I_2 \times I_3$ is decomposed to the product of the core tensor \mathcal{S} of size $J_1 \times J_2 \times J_3$ and factor matrices $\mathbf{A}^{(1)}$, $\mathbf{A}^{(2)}$, and $\mathbf{A}^{(3)}$.

A pruning approach (Han et al., 2015b;a) also aims at reducing the total amount of parameters and operations in the entire network. Pruning based approaches can give significant reductions in parameter size and computation workload. However, it is challenging to achieve runtime speed-up with conventional GPU implementation as mentioned in (Han et al., 2015a).

Orthogonal to model level compression, implementation level approaches were also proposed. The FFT method was used to speed-up convolution (Mathieu et al., 2013). In (Vanhoecke et al., 2011), CPU code optimizations to speed-up the execution of CNN are extensively explored.

2.2 TENSOR DECOMPOSITION

A tensor is a multi-way array of data. For example, a vector is 1-way tensor and a matrix is 2-way tensor. Two of the most popular tensor decomposition models are CANDECOMP/PARAFAC model (Carroll & Chang, 1970; Harshman & Lundy, 1994; Shashua & Hazan, 2005) and Tucker model (Tucker, 1966; De Lathauwer et al., 2000; Kim & Choi, 2007). In this paper, we extensively use Tucker model for whole network compression. Tucker decomposition is a higher order extension of the singular value decomposition (SVD) of matrix, in the perspective of computing the orthonormal spaces associated with the different modes of a tensor. It simultaneously analyzes mode- n matricizations of the original tensor, and merges them with the core tensor as illustrated in Fig. 1.

In our whole network compression scheme, we apply Tucker-2 decomposition, which is also known as GLRAM (Ye, 2005), from the second convolutional layer to the first fully connected layers. For the other layers, we apply Tucker-1 decomposition, which is equivalent to SVD. For more information on the tensor decomposition, the reader is referred to the survey paper (Kolda & Bader, 2009).

3 PROPOSED METHOD

Fig. 2 illustrates our one-shot whole network compression scheme which consists of three steps: (1) rank selection; (2) Tucker decomposition; (3) fine-tuning. In the first step, we analyze principal subspace of mode-3 and mode-4 matricization of each layer’s kernel tensor with global analytic variational Bayesian matrix factorization. Then we apply Tucker decomposition on each layer’s kernel tensor with previously determined rank. Finally, we fine-tune the entire network with standard back-propagation.

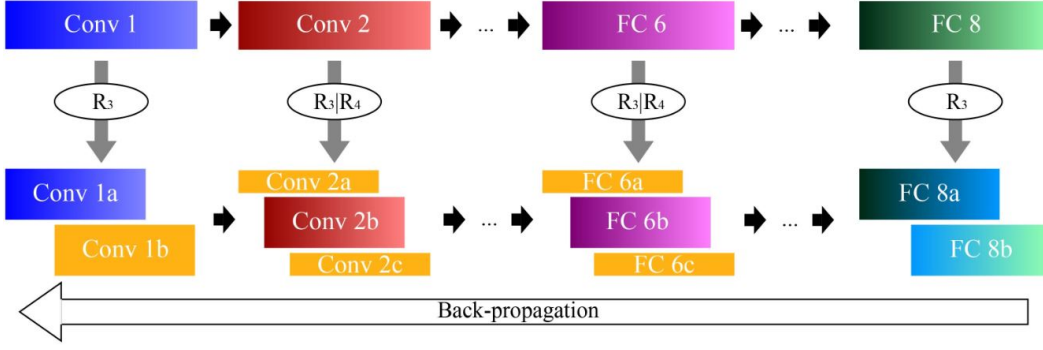


Figure 2: Our one-shot whole network compression scheme consists of (1) rank selection with VBMF; (2) Tucker decomposition on kernel tensor; (3) fine-tuning of entire network. **Note that Tucker-2 decomposition is applied from the second convolutional layer to the first fully connected layers, and Tucker-1 decomposition to the other layers.**

3.1 TUCKER DECOMPOSITION ON KERNEL TENSOR

Convolution kernel tensor: In CNNs, the convolution operation maps an input (source) tensor \mathcal{X} of size $H \times W \times S$ into output (target) tensor \mathcal{Y} of size $H' \times W' \times T$ using the following linear mapping:

$$\mathcal{Y}_{h',w',t} = \sum_{i=1}^D \sum_{j=1}^D \sum_{s=1}^S \mathcal{K}_{i,j,s,t} \mathcal{X}_{h_i,w_j,s},$$

$$h_i = (h' - 1)\Delta + i - P \text{ and } w_j = (w' - 1)\Delta + j - P, \quad (1)$$

where \mathcal{K} is a 4-way kernel tensor of size $D \times D \times S \times T$, Δ is stride, and P is zero-padding size.

Tucker Decomposition: The rank- (R_1, R_2, R_3, R_4) Tucker decomposition of 4-way kernel tensor \mathcal{K} has the form:

$$\mathcal{K}_{i,j,s,t} = \sum_{r_1=1}^{R_1} \sum_{r_2=1}^{R_2} \sum_{r_3=1}^{R_3} \sum_{r_4=1}^{R_4} \mathcal{C}'_{r_1,r_2,r_3,r_4} U_{i,r_1}^{(1)} U_{j,r_2}^{(2)} U_{s,r_3}^{(3)} U_{t,r_4}^{(4)},$$

where \mathcal{C}' is a core tensor of size $R_1 \times R_2 \times R_3 \times R_4$ and $U^{(1)}$, $U^{(2)}$, $U^{(3)}$, and $U^{(4)}$ are factor matrices of sizes $D \times R_1$, $D \times R_2$, $S \times R_3$, and $T \times R_4$, respectively.

In the Tucker decomposition, every mode does not have to be decomposed. For example, **we do not decompose mode-1 and mode-2 which are associated with spatial dimensions because they are already quite small** (D is typically 3 or 5). Under this variant called Tucker-2 decomposition (Tucker, 1966), the kernel tensor is decomposed to:

$$\mathcal{K}_{i,j,s,t} = \sum_{r_3=1}^{R_3} \sum_{r_4=1}^{R_4} \mathcal{C}_{i,j,r_3,r_4} U_{s,r_3}^{(3)} U_{t,r_4}^{(4)}, \quad (2)$$

where \mathcal{C} is a core tensor of size $D \times D \times R_3 \times R_4$. After substituting (2) into (1), **performing rearrangements and grouping summands**, we obtain the following three consecutive expressions for the approximate evaluation of the convolution (1):

$$\mathcal{Z}_{h,w,r_3} = \sum_{s=1}^S U_{s,r_3}^{(3)} \mathcal{X}_{h,w,s}, \quad (3)$$

$$\mathcal{Z}'_{h',w',r_4} = \sum_{i=1}^D \sum_{j=1}^D \sum_{r_3=1}^{R_3} \mathcal{C}_{i,j,r_3,r_4} \mathcal{Z}_{h_i,w_j,r_3}, \quad (4)$$

$$\mathcal{Y}_{h',w',t} = \sum_{r_4=1}^{R_4} U_{t,r_4}^{(4)} \mathcal{Z}'_{h',w',r_4}, \quad (5)$$

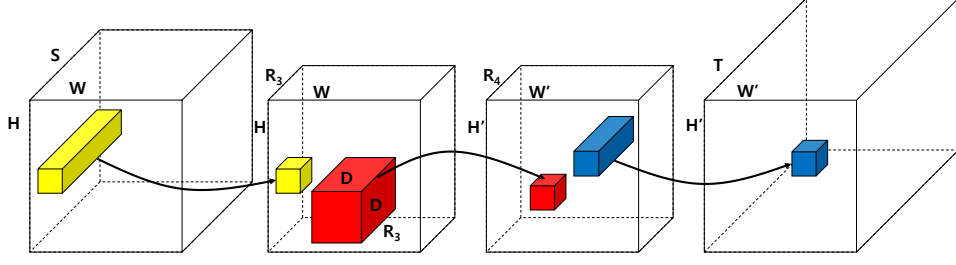


Figure 3: Tucker-2 decompositions for speeding-up a convolution. Each transparent box corresponds to 3-way tensor \mathcal{X} , \mathcal{Z} , \mathcal{Z}' , and \mathcal{Y} in (3-5), with two frontal sides corresponding to spatial dimensions. Arrows represent linear mappings and illustrate how scalar values on the right are computed. Yellow tube, red box, and blue tube correspond to 1×1 , $D \times D$, and 1×1 convolution in (3), (4), and (5) respectively.

where \mathcal{Z} and \mathcal{Z}' are intermediate tensors of sizes $H \times W \times R_3$ and $H' \times W' \times R_4$, respectively.

1×1 convolution: As illustrated in Fig. 3, computing \mathcal{Z} from \mathcal{X} in (3) as well as \mathcal{Y} from \mathcal{Z}' in (5) is 1×1 convolutions that essentially perform pixel-wise linear re-combination of input maps. It is introduced in *network-in-network* (Lin et al., 2014) and extensively used in *inception* module of *GoogLeNet* (Szegedy et al., 2015). Note that computing (3) is similar to inception module in the sense that $D \times D$ convolution is applied after dimensional reduction with 1×1 convolution, but different in the sense that there is no non-linear *ReLU* function between (3) and (4). In addition, similar to (Zhang et al., 2015b;a), we compute smaller intermediate output tensor \mathcal{Z}' in (4) and then recover its size in (5). The Tucker-2 decomposition naturally integrates two compression techniques.

Complexity analysis: The convolution operation in (1) requires D^2ST parameters and $D^2STH'W'$ multiplication-addition operations. With Tucker decomposition, compression ratio M and speed-up ratio E are given by:

$$M = \frac{D^2ST}{SR_3 + D^2R_3R_4 + TR_4} \quad \text{and} \quad E = \frac{D^2STH'W'}{SR_3HW + D^2R_3R_4H'W' + TR_4H'W'},$$

and these are bounded by ST/R_3R_4 .

Tucker vs CP: Recently, CP decomposition is applied to approximate the convolution layers of CNNs for *ImageNet* which consist of 8 layers (Denton et al., 2014; Lebedev et al., 2015). However it cannot be applied to the entire layers and the instability issue of low-rank CP decomposition is reported (De Silva & Lim, 2008; Lebedev et al., 2015). On the other hand, our kernel tensor approximation with Tucker decomposition can be successfully applied to the entire layers of *AlexNet*, *VGG-S*, *GoogLeNet*, and *VGG-16*.

3.2 RANK SELECTION WITH GLOBAL ANALYTIC VBMF

The rank- (R_3, R_4) are very important hyper-parameters which control the trade-off between performance (memory, speed, energy) improvement and accuracy loss. Instead of selecting the rank- (R_3, R_4) by time consuming trial-and-error, we considered data-driven one-shot decision via *empirical Bayes* (MacKay, 1992) with *automatic relevance determination* (ARD) prior (Tipping, 2001).

At the first time, we designed probabilistic Tucker model which is similar to (Mørup & Hansen, 2009), and applied empirical variational Bayesian learning. However, the rank selection results were severely unreliable because they heavily depend on (1) initial condition, (2) noise variance estimation policy, and (3) threshold setting for pruning. For this reason, we decided to use a sub-optimal but highly reproducible approach.

We employed recently developed global analytic solutions for variational Bayesian matrix factorization (VBMF) (Nakajima et al., 2013). The global analytic VBMF is a very promising tool because it can automatically find noise variance, rank and even provide theoretical condition for perfect rank recovery (Nakajima et al., 2012). We determined the rank R_3 and R_4 by applying global analytic VBMF on mode-3 matricization (of size $S \times TD^2$) and mode-4 matricization (of size $T \times D^2S$) of kernel tensor \mathcal{K} , respectively.

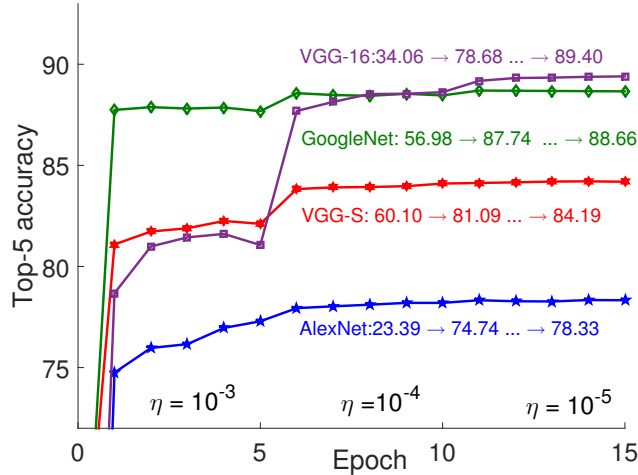


Figure 4: Accuracy of compressed CNNs in fine-tuning.

3.3 FINE-TUNING

Because we minimize the reconstruction error of linear kernel tensors instead of non-linear responses, the accuracy is significantly dropped after whole network compression (e.g. more than 50% in the case of *AlexNet*). However, as shown in Fig. 4, we can easily recover the accuracy by using fine-tuning with *ImageNet* training dataset. We observed that accuracy is recovered quickly in one epoch. However, more than 10 epochs are required to recover the original accuracy.

While (Lebedev et al., 2015; Zhang et al., 2015a) reported difficulty on finding a good SGD learning rate, our single learning rate scheduling rule works well for various compressed CNNs. In our experiment, we set the base learning $\eta = 10^{-3}$ and decrease it by a factor of 10 every 5 epochs. Because of GPU memory limitation, we set the batch size: 128, 128, 64, and 32 for *AlexNet*, *VGG-S*, *GoogLeNet*, and *VGG-16*, respectively.

We also tried to train the architecture of the approximated model from scratch on the *ImageNet* training dataset. At this time, we only tested the Gaussian random initialization and it did not work. We leave the use of other initialization methods (Glorot & Bengio, 2010; He et al., 2015) and *batch normalization* (Ioffe & Szegedy, 2015) as future work.

4 EXPERIMENTS

We used four representative CNNs, *AlexNet*, *VGG-S*, *GoogLeNet*, and *VGG-16*, which can be downloaded on Berkeley’s *Caffe model zoo*. In the case of *inception* module of *GoogLeNet*, we only compressed the 3×3 convolution kernel which is the main computational part. In the case of *VGG-16*, we only compressed the convolutional layers as done in (Zhang et al., 2015a). Top-5 single-view accuracy is measured using 50,000 validation images from the *ImageNet2012* dataset.

We performed experiments on Nvidia Titan X (for fine-tuning and runtime comparison on Caffe+cuDNN2) and a smartphone, Samsung Galaxy S6 (for the comparison of runtime and energy consumption). The application processor of the smartphone (Exynos 7420) is equipped with a mobile GPU, ARM Mali T760. Compared with the GPU used on Titan X, the mobile GPU gives 35 times (6.6TFlops vs 190GFlops) lower computing capability and 13 times (336.5GBps vs 25.6GBps) smaller memory bandwidth.

In order to run Caffe models on the mobile GPU, we developed a mobile version of Caffe called S-Caffe (Caffe for Smart mobile devices) where all the Caffe models can run on our target mobile devices (for the moment, Samsung smartphones) without modification. We also developed an Android App which performs image classification by running each of the four CNNs (*AlexNet*, *VGG-S*, *GoogLeNet*, and *VGG-16*) on the smartphone.

We measured the power consumption of whole smartphone which is decomposed into the power consumption of GPU, main memory, and the other components of smartphone, e.g., ARM CPU, display, modem, etc. and give component-level analysis, especially, the power consumption of GPU and main memory (see supplementary material for details of measurement environment). The measurement results of runtime and energy consumption are the average of 50 runs.

4.1 OVERALL RESULTS

Table 1 shows the overall results for the three CNNs. Our proposed scheme gives $\times 5.46 / \times 2.67$ (*AlexNet*), $\times 7.40 / \times 4.80$ (*VGG-S*), $\times 1.28 / \times 2.06$ (*GoogLeNet*), and $\times 1.09 / \times 4.93$ (*VGG-16*) reductions in total weights and FLOPs, respectively. Such reductions offer $\times 1.42 \sim \times 3.68$ ($\times 1.23 \sim \times 2.33$) runtime improvements on the smartphone (Titan X). We report the energy consumption of mobile GPU and main memory. The smartphone gives larger reduction ratios (e.g., $\times 3.41$ vs. $\times 2.72$ for *AlexNet*) for energy consumption than runtime. We will give a detailed analysis in the following subsection.

Comparison with Zhang et al. (2015a)’s method: The accuracy of our compressed *VGG-16* is 89.40% for theoretical $\times 4.93$ speed-up, and it is comparable to the 89.6% (88.9%) for theoretical $\times 4$ ($\times 5$) speed-up in (Zhang et al., 2015a).

Table 1: Original versus compressed CNNs. Memory, runtime and energy are significantly reduced with only minor accuracy drop. We report the time and energy consumption for processing single image in S6 and Titan X. (* compression, S6: Samsung Galaxy S6).

Model	Top-5	Weights	FLOPs	S6		Titan X
<i>AlexNet</i>	80.03	61M	725M	117ms	245mJ	0.54ms
<i>AlexNet</i> *	78.33	11M	272M	43ms	72mJ	0.30ms
(imp.)	(-1.70)	($\times 5.46$)	($\times 2.67$)	($\times 2.72$)	($\times 3.41$)	($\times 1.81$)
<i>VGG-S</i>	84.60	103M	2640M	357ms	825mJ	1.86ms
<i>VGG-S</i> *	84.05	14M	549M	97ms	193mJ	0.92ms
(imp.)	(-0.55)	($\times 7.40$)	($\times 4.80$)	($\times 3.68$)	($\times 4.26$)	($\times 2.01$)
<i>GoogLeNet</i>	88.90	6.9M	1566M	273ms	473mJ	1.83ms
<i>GoogLeNet</i> *	88.66	4.7M	760M	192ms	296mJ	1.48ms
(imp.)	(-0.24)	($\times 1.28$)	($\times 2.06$)	($\times 1.42$)	($\times 1.60$)	($\times 1.23$)
<i>VGG-16</i>	89.90	138M	15484M	1926ms	4757mJ	10.67ms
<i>VGG-16</i> *	89.40	127M	3139M	576ms	1346mJ	4.58ms
(imp.)	(-0.50)	($\times 1.09$)	($\times 4.93$)	($\times 3.34$)	($\times 3.53$)	($\times 2.33$)

4.2 LAYERWISE ANALYSIS

Tables 2, 3, 4 and 5¹ show the detailed comparisons. Each row has two results (the above one for the original uncompressed CNN and the other one for the compressed CNN), and improvements. For instance, in Table 2, the second convolutional layer having the input and output channel dimensions of 48×2 and 128×2 is compressed to give the Tucker-2 ranks of 25×2 and 59×2 , which reduces the amount of weights from 307K to 91K. After compression, a layer in the compressed network performs three matrix multiplications. We give the details of three matrix multiplications for each of weights, FLOPs, and runtime. For instance, on the smartphone (column S6 in Table 2), the second convolutional layer of compressed *AlexNet* takes 10.53ms which is decomposed to 0.8ms, 7.43ms and 2.3ms for the three matrix multiplications.

In Tables 2, 3, 4 and 5 we have two observations.

Observation 1: Given a compressed network, the smartphone tends to give larger performance gain than the Titan X. It is mainly because the mobile GPU on the smartphone lacks in thread-level parallelism. It has 24 times less number of threads (2K vs. 48K in terms of maximum number of threads) than that in Titan X. Compression reduces the amount of weights thereby reducing cache conflicts and memory latency. Due to the small thread-level parallelism, the reduced latency has more impact on the performance of threads on the mobile GPU than that on Titan X.

¹See supplementary material for Tables 3, 4 and 5

Table 2: Layerwise analysis on *AlexNet*. Note that conv2, conv4, and conv5 layer have 2-group structure. (S : input channel dimension, T : output channel dimension, (R_3, R_4): Tucker-2 rank).

Layer	S/R_3	T/R_4	Weights	FLOPs	S6
conv1	3	96	35K	105M	15.05 ms
conv1* (imp.)		26	11K ($\times 2.92$)	36M(=29+7) ($\times 2.92$)	10.19m(=8.28+1.90) ($\times 1.48$)
conv2	48×2	128×2	307K	224M	24.25 ms
conv2* (imp.)	25×2	59×2	91K ($\times 3.37$)	67M(=2+54+11) ($\times 3.37$)	10.53ms(=0.80+7.43+2.30) ($\times 2.30$)
conv3	256	384	885K	150M	18.60ms
conv3* (imp.)	105	112	178K ($\times 5.03$)	30M(=5+18+7) ($\times 5.03$)	4.85ms(=1.00+2.72+1.13) ($\times 3.84$)
conv4	192×2	192×2	664K	112M	15.17ms
conv4* (imp.)	49×2	46×2	77K ($\times 7.10$)	13M(=3+7+3) ($\times 7.10$)	4.29 ms(=1.55+1.89+0.86) ($\times 3.53$)
conv5	192×2	128×2	442K	75.0M	10.78ms
conv5* (imp.)	40×2	34×2	49K ($\times 9.11$)	8.2M(=2.6+4.1+1.5) ($\times 9.11$)	3.44 ms(=1.15+1.61+0.68) ($\times 3.13$)
fc6	256	4096	37.7M	37.7M	18.94ms
fc6* (imp.)	210	584	6.9M ($\times 8.03$)	8.7M(=1.9+4.4+2.4) ($\times 4.86$)	5.07 ms(=0.85+3.12+1.11) ($\times 3.74$)
fc7	4096	4096	16.8M	16.8M	7.75ms
fc7* (imp.)		301	2.4M ($\times 6.80$)	2.4M(=1.2+1.2) ($\times 6.80$)	1.02 ms(=0.51+0.51) ($\times 7.61$)
fc8	4096	1000	4.1M	4.1M	2.00ms
fc8* (imp.)		195	1.0M ($\times 4.12$)	1.0M(=0.8+0.2) ($\times 4.12$)	0.66ms(=0.44+0.22) ($\times 3.01$)

Observation 2: Given the same compression rate, the smartphone tends to exhibit larger performance gain at fully-connected layers than at convolutional layers. We think it is also due to the reduced cache conflicts enabled by network compression as explained above. Especially, in the case of fully-connected layers, the effect of weight reduction can give more significant impact because the weights at the fully-connected layers are utilized only once, often called dead-on-arrival (DoA) data. In terms of cache performance, such DoA data are much more harmful than convolution kernel weights (which are reused multiple times). Thus, weight reduction at the fully connected layer can give more significant impact on cache performance thereby exhibiting more performance improvement than in the case of weight reduction at convolutional layers.

4.3 ENERGY CONSUMPTION ANALYSIS

Fig. 5 compares power consumption on the smartphone. Each network gives the power consumption of GPU and main memory. Note that we enlarged the time axis of compressed networks for a better comparison. We omitted *VGG-16* since *VGG-16* gives similar trend.

The figure shows that the compression reduces power consumption (Y axis) as well as runtime (X axis), which explains why the reduction in energy consumption is larger than that in runtime in Table 1. Fig. 5 also shows that the GPU power consumption of compressed CNN is smaller than that of uncompressed CNN. We analyze this due to the extensive usage of 1×1 convolutions in the compressed CNN. When executing convolutions, we apply optimization techniques such as *Caffeinated convolution* (Chellapilla et al., 2006). In such a case, in terms of cache efficiency, 1×1 convolutions are inferior to the other convolutions, e.g., 3×3 , 5×5 , etc. since the amount of data reuse is proportional to the total size of convolution kernel. Thus, 1×1 convolutions tend to incur more cache misses than the other larger convolutions. Cache misses on the mobile GPU without sufficient thread level parallelism often incur stall cycles, i.e., make GPU cores idle consuming less power, which reduces the power consumption of GPU core during the execution of 1×1 convolution.

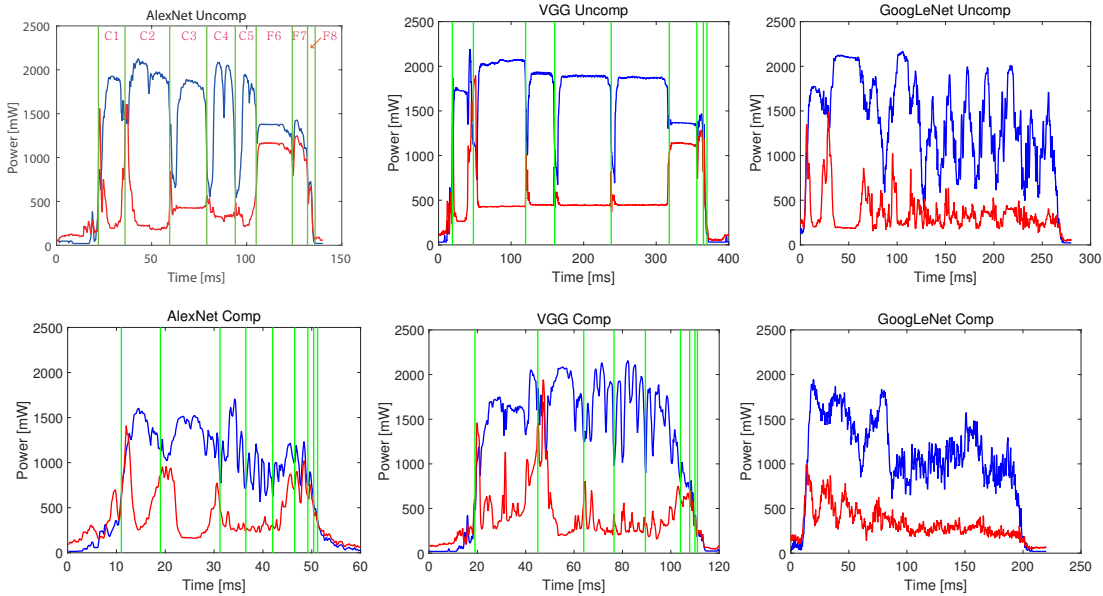


Figure 5: Power consumption over time for each model. (Blue: GPU, Red: main memory).

As mentioned earlier, our proposed method improves cache efficiency by reducing the amount of weights. However, 1×1 convolutions have negative impacts on cache efficiency and GPU core utilization. Fig. 5 shows the combined effects. In the compressed networks, the power consumption of GPU core is reduced by 1×1 convolutions and tends to change more frequently due to frequent executions of 1×1 convolution while, in the case of uncompressed networks, especially for *AlexNet* and *VGG-S*, the power consumption of GPU core tends to be stable during the execution of convolutional layers. In the case of uncompressed *GoogLeNet*, the power consumption tends to fluctuate. It is mainly because (1) *GoogLeNet* consists of many small layers (about 100 building blocks), and (2) 1×1 convolutions are heavily utilized.

The three compressed networks show similar behavior of frequent fluctuations in power consumption mostly due to 1×1 convolutions. Fig. 5 also shows that, in the uncompressed networks, fully connected layers incur significant amount of power consumption in main memory. It is because the uncompressed networks, especially *AlexNet* and *VGG-S* have large numbers (more than tens of mega-bytes) of weights in fully connected layers which incur significant amount of memory accesses. As shown in Fig. 5, the proposed scheme reduces the amount of weights at fully connected layers thereby reducing the power consumption in main memory.

5 DISCUSSION

Although we can obtain very promising results with one-shot rank selection, it is not fully investigated yet whether the selected rank is really optimal or not. As future work, we will investigate the optimality of our proposed scheme. The 1×1 convolution is a key operation in our compressed model as well as in *inception* module of *GoogLeNet*. Due to its characteristics, e.g. channel compression and computation reduction, we expect that 1×1 convolutions will become more and more popular in the future. However, as shown in our experimental results, it lacks in cache efficiency. We expect further investigations are required to make best use of 1×1 convolutions.

Whole network compression is challenging due to the large design space and associated long design time. In order to address this problem, we propose a one-shot compression scheme which applies a single general low-rank approximation method and a global rank selection method. Our one-shot compression enables fast design and easy implementation with publicly available tools. We evaluated the effectiveness of the proposed scheme on a smartphone and Titan X. The experiments show that the proposed scheme gives, for four CNNs (*AlexNet*, *VGG-S*, *GoogLeNet*, and *VGG-16*) average $\times 2.72$ ($\times 3.41$), $\times 3.68$ ($\times 4.26$), $\times 1.42$ ($\times 1.60$), and $\times 3.34$ ($\times 3.53$) improvements in runtime (energy consumption) on the smartphone.

REFERENCES

- Bader, Brett W., Kolda, Tamara G., et al. Matlab tensor toolbox version 2.6. Available online, February 2015. URL <http://www.sandia.gov/~tgkolda/TensorToolbox/>.
- Carroll, J Douglas and Chang, Jih-Jie. Analysis of individual differences in multidimensional scaling via an n-way generalization of eckart-young decomposition. *Psychometrika*, 35(3):283–319, 1970.
- Chellapilla, Kumar, Puri, Sidd, and Simard, Patrice. High performance convolutional neural networks for document processing. In *Tenth International Workshop on Frontiers in Handwriting Recognition*. Suvisoft, 2006.
- Chen, Wenlin, Wilson, James T, Tyree, Stephen, Weinberger, Kilian Q, and Chen, Yixin. Compressing neural networks with the hashing trick. *arXiv preprint arXiv:1504.04788*, 2015.
- Cheng, Yu, Yu, Felix X, Feris, Rogerio S, Kumar, Sanjiv, Choudhary, Alok, and Chang, Shih-Fu. Fast neural networks with circulant projections. *arXiv preprint arXiv:1502.03436*, 2015.
- De Lathauwer, Lieven, De Moor, Bart, and Vandewalle, Joos. A multilinear singular value decomposition. *SIAM journal on Matrix Analysis and Applications*, 21(4):1253–1278, 2000.
- De Silva, Vin and Lim, Lek-Heng. Tensor rank and the ill-posedness of the best low-rank approximation problem. *SIAM Journal on Matrix Analysis and Applications*, 30(3):1084–1127, 2008.
- Denil, Misha, Shakibi, Babak, Dinh, Laurent, de Freitas, Nando, et al. Predicting parameters in deep learning. In *Advances in Neural Information Processing Systems*, pp. 2148–2156, 2013.
- Denton, Emily L, Zaremba, Wojciech, Bruna, Joan, LeCun, Yann, and Fergus, Rob. Exploiting linear structure within convolutional networks for efficient evaluation. In *Advances in Neural Information Processing Systems*, pp. 1269–1277, 2014.
- Glorot, Xavier and Bengio, Yoshua. Understanding the difficulty of training deep feedforward neural networks. In *International conference on artificial intelligence and statistics*, pp. 249–256, 2010.
- Gong, Yunchao, Liu, Liu, Yang, Ming, and Bourdev, Lubomir. Compressing deep convolutional networks using vector quantization. *arXiv preprint arXiv:1412.6115*, 2014.
- Han, Song, Mao, Huizi, and Dally, William J. A deep neural network compression pipeline: Pruning, quantization, huffman encoding. *arXiv preprint arXiv:1510.00149*, 2015a.
- Han, Song, Pool, Jeff, Tran, John, and Dally, William J. Learning both weights and connections for efficient neural networks. *arXiv preprint arXiv:1506.02626*, 2015b.
- Harshman, Richard A and Lundy, Margaret E. Parafac: Parallel factor analysis. *Computational Statistics & Data Analysis*, 18(1):39–72, 1994.
- He, Kaiming, Zhang, Xiangyu, Ren, Shaoqing, and Sun, Jian. Delving deep into rectifiers: Surpassing human-level performance on imagenet classification. In *IEEE International Conference on Computer Vision*, 2015.
- Hinton, Geoffrey E, Srivastava, Nitish, Krizhevsky, Alex, Sutskever, Ilya, and Salakhutdinov, Ruslan R. Improving neural networks by preventing co-adaptation of feature detectors. *arXiv preprint arXiv:1207.0580*, 2012.
- Ioffe, Sergey and Szegedy, Christian. Batch normalization: Accelerating deep network training by reducing internal covariate shift. In *International Conference on Machine Learning*, 2015.
- Jaderberg, M., Vedaldi, A., and Zisserman, A. Speeding up convolutional neural networks with low rank expansions. In *British Machine Vision Conference*, 2014.
- Kim, Y.-D. and Choi, S. Nonnegative Tucker decomposition. In *Proceedings of the IEEE CVPR-2007 Workshop on Component Analysis Methods*, Minneapolis, Minnesota, 2007.

- Kolda, Tamara G and Bader, Brett W. Tensor decompositions and applications. *SIAM review*, 51(3): 455–500, 2009.
- Lebedev, Vadim, Ganin, Yaroslav, Rakhuba, Maksim, Oseledets, Ivan, and Lempitsky, Victor. Speeding-up convolutional neural networks using fine-tuned cp-decomposition. In *International Conference on Learning Representations*, 2015.
- Lin, M., Chen, Q., and Yan, S. Network in network. In *International Conference on Learning Representations*, 2014.
- MacKay, David JC. Bayesian interpolation. *Neural computation*, 4(3):415–447, 1992.
- Mathieu, Michael, Henaff, Mikael, and LeCun, Yann. Fast training of convolutional networks through ffts. *arXiv preprint arXiv:1312.5851*, 2013.
- Mørup, Morten and Hansen, Lars Kai. Automatic relevance determination for multi-way models. *Journal of Chemometrics*, 23(7-8):352–363, 2009.
- Nakajima, Shinichi. *Variational Bayesian matrix factorization version 1.02*, 2015. URL <https://sites.google.com/site/shinnkj23/downloads>.
- Nakajima, Shinichi, Tomioka, Ryota, Sugiyama, Masashi, and Babacan, S Derin. Perfect dimensionality recovery by variational bayesian pca. In *Advances in Neural Information Processing Systems*, pp. 971–979, 2012.
- Nakajima, Shinichi, Sugiyama, Masashi, Babacan, S Derin, and Tomioka, Ryota. Global analytic solution of fully-observed variational bayesian matrix factorization. *The Journal of Machine Learning Research*, 14(1):1–37, 2013.
- Novikov, Alexander, Podoprikin, Dmitry, Osokin, Anton, and Vetrov, Dmitry. Tensorizing neural networks. *arXiv preprint arXiv:1509.06569*, 2015.
- Shashua, Amnon and Hazan, Tamir. Non-negative tensor factorization with applications to statistics and computer vision. In *Proceedings of the 22nd international conference on Machine learning*, pp. 792–799. ACM, 2005.
- Simonyan, K. and Zisserman, A. Very deep convolutional networks for large-scale image recognition. In *International Conference on Learning Representations*, 2015.
- Szegedy, Christian, Liu, Wei, Jia, Yangqing, Sermanet, Pierre, Reed, Scott, Anguelov, Dragomir, Erhan, Dumitru, Vanhoucke, Vincent, and Rabinovich, Andrew. Going deeper with convolutions. In *IEEE Conference on Computer Vision and Pattern Recognition (CVPR)*, 2015.
- Tipping, Michael E. Sparse bayesian learning and the relevance vector machine. *The journal of machine learning research*, 1:211–244, 2001.
- Tucker, Ledyard R. Some mathematical notes on three-mode factor analysis. *Psychometrika*, 31(3): 279–311, 1966.
- Vanhoucke, Vincent, Senior, Andrew, and Mao, Mark Z. Improving the speed of neural networks on cpus. In *Proc. Deep Learning and Unsupervised Feature Learning NIPS Workshop*, volume 1, 2011.
- Ye, Jieping. Generalized low rank approximations of matrices. *Machine Learning*, 61(1-3):167–191, 2005.
- Zhang, Xiangyu, Zou, Jianhua, He, Kaiming, and Sun, Jian. Accelerating very deep convolutional networks for classification and detection. *arXiv preprint arXiv:1505.06798*, 2015a.
- Zhang, Xiangyu, Zou, Jianhua, Ming, Xiang, He, Kaiming, and Sun, Jian. Efficient and accurate approximations of nonlinear convolutional networks. 2015b.

APPENDICES

A EXPERIMENTAL SETUP

This section describes the details of experimental setup including the measurement system for power consumption and exemplifies the measured data.

A.1 MEASUREMENT SYSTEM

Fig. 6 shows the power measurement system. As the figure shows, it consists of a probe board (left) having a Samsung Galaxy S6 smartphone and power probes and a monitor board (right). The probe board provides 8 probes which are connected to the power pins of application processor (to be introduced below). The power profiling monitor samples, for each power probe, the electric current every 0.1ms and gives power consumption data with time stamps.

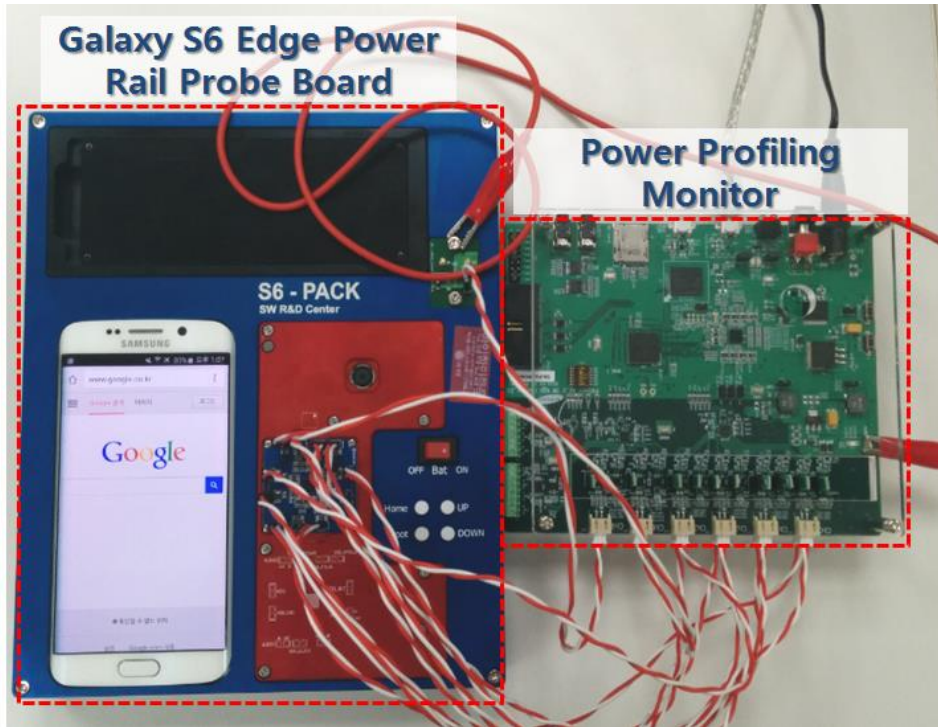


Figure 6: Power measurement system.

Fig. 7 illustrates the main board of the smartphone (Fig. 7 (a)), the application processor chip package (red rectangle in Fig. 2 (a)) consisting of the application processor and main memory (LPDDR4 DRAM) in the smartphone (Fig. 7 (b)), and a simplified block diagram of the application processor (Fig. 7 (c)). The power measurement system provides the probes connected to the power pins for mobile GPU (ARM Mali T760 in Fig. 7 (c)) and main memory (LPDDR4 DRAM in Fig. 7 (b)).

A.2 MEASURED DATA EXAMPLE: *GoogLeNet* CASE

Fig. 8 shows the power consumption data for the uncompressed GoogLeNet. We also identified the period of each layer, e.g., the first convolutional layer (Conv 1 in the figure), and the first Inception module (i3a). As mentioned in our submission, the profile of power consumption shows more frequent fluctuations in Inception modules than in the convolutional layers. The figure also shows that the first two convolutional layers (Conv 1 and Conv 2) occupy about 1/4 of total energy consumption while Inception modules consume about 3/4 of total energy consumption.

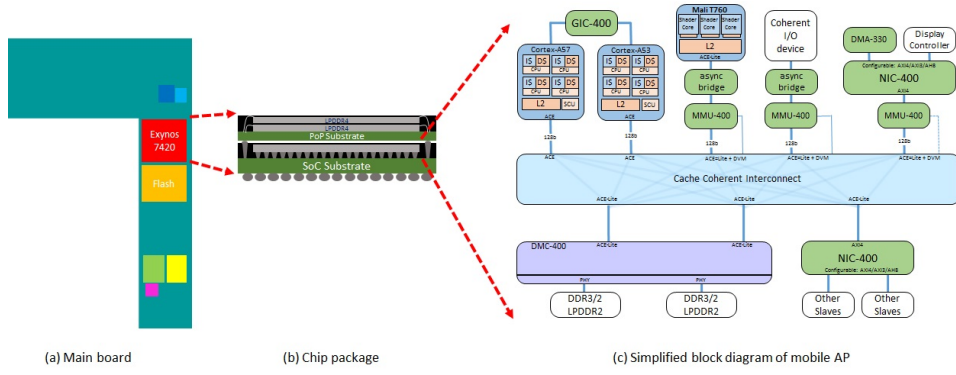
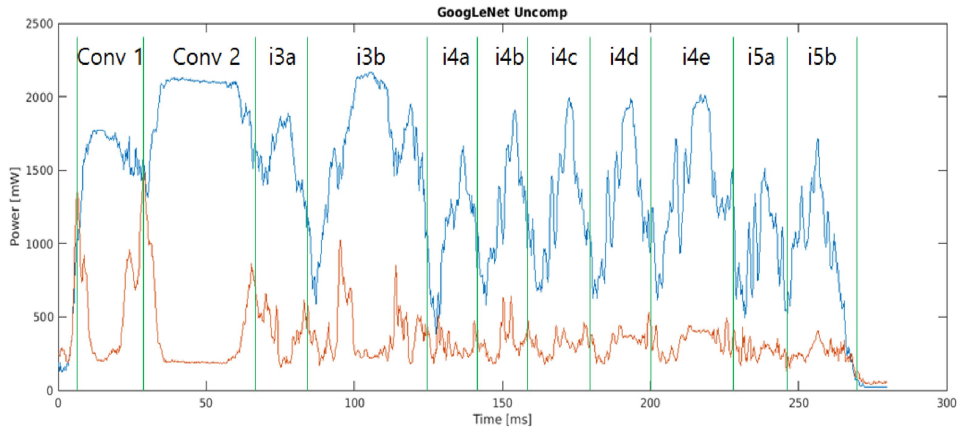


Figure 7: Details of mobile application processor and main memory.

Figure 8: Power profile of uncompressed *GoogLeNet*.

B LAYERWISE ANALYSIS

We report detailed comparison results *VGG-S*, *GoogLeNet*, and *VGG-16*.

Table 3: Layerwis analysis on VGG-S. (S : input channel dimension, T : output channel dimension, (R_3, R_4): Tucker-2 rank).

Layer	S/R_3	T/R_4	Weights	FLOPs	S6
conv1	3	96	14K	168M	23.88ms
conv1* (imp.)		42	10K ($\times 1.38$)	121M(=73+48) ($\times 1.38$)	23.15ms(=14.47+8.68) ($\times 1.03$)
conv2	96	256	614K	699M	74.57ms
conv2* (imp.)	48	89	134K ($\times 4.58$)	147M(=6+116+25) ($\times 4.54$)	18.54ms(=1.32+13.59+3.64) ($\times 4.02$)
conv3	256	512	1180K	341M	38.33ms
conv3* (imp.)	126	175	320K ($\times 3.68$)	93M(=9+57+26) ($\times 3.68$)	11.59ms(=1.53+6.82+3.24) ($\times 3.31$)
conv4	512	512	2359K	682M	78.43ms
conv4* (imp.)	143	144	332K ($\times 7.10$)	96M(=21+54+21) ($\times 7.10$)	12.23ms(=2.92+6.63+2.78) ($\times 6.37$)
conv5	512	512	2359K	682M	78.40ms
conv5* (imp.)	120	120	252K ($\times 9.34$)	73M(=18+37+18) ($\times 9.34$)	10.25ms(=2.76+5.03+2.46) ($\times 7.65$)
fc6	512	4096	75.5M	75.5M	40.75ms
fc6* (imp.)	343	561	9.4M ($\times 8.03$)	15.5M(=6.3+6.9+2.3) ($\times 4.86$)	7.18ms(=1.58+4.61+0.98) ($\times 5.68$)
fc7	4096	4096	16.8M	16.8M	7.68ms
fc7* (imp.)		301	2.4M ($\times 6.80$)	2.4M(=1.2+1.2) ($\times 6.80$)	1.26ms(=0.65+0.60) ($\times 6.10$)
fc8	4096	1000	4.1M	4.1M	1.97ms
fc8* (imp.)		195	1.0M ($\times 4.12$)	1.0M(=0.8+0.2) ($\times 4.12$)	0.67ms(=0.45+0.22) ($\times 2.92$)

Table 4: Layerwise analysis on *GoogLeNet*. (S : input channel dimension, T : output channel dimension, (R_3, R_4) : Tucker-2 rank).

Layer	S/R_3	T/R_4	Weights	FLOPs	S6
conv1	3	64	9.4K	118M	18.96ms
conv1* (imp.)		23	4.8K ($\times 1.94$)	60M(=42+18) ($\times 1.94$)	21.76ms(=16.85+4.91) ($\times 0.87$)
conv2	64	192	11.1K	347M	34.69ms
conv2* (imp.)		23	4.8K ($\times 4.99$)	60M(=42+18) ($\times 4.99$)	12.04ms(=1.66+5.95+4.43) ($\times 2.88$)
i3a	96	128	111K(68%)	87M(68%)	9.39ms
i3a* (imp.)	41	41	24K ($\times 4.55$)	19M(3+12+4) ($\times 4.55$)	3.70ms=(0.70+2.02+0.98) ($\times 2.54$)
i3b	128	192	221K(57%)	173M(57%)	17.49ms
i3b* (imp.)	42	37	26K ($\times 8.36$)	21M(4+11+6) ($\times 8.36$)	4.10ms=(0.89+1.99+1.21) ($\times 4.27$)
i4a	96	208	180K(48%)	35M(48%)	4.35ms
i4a* (imp.)	35	39	24K ($\times 7.56$)	5M(1+2+2) ($\times 7.56$)	1.68ms=(0.39+0.79+0.50) ($\times 2.60$)
i4b	112	224	226K(51%)	44M(51%)	5.39ms
i4b* (imp.)	55	75	60K ($\times 3.76$)	12M(1+7+3) ($\times 3.76$)	2.65ms=(0.47+1.48+0.70) ($\times 2.03$)
i4c	128	256	295K(58%)	58M(58%)	6.93ms
i4c* (imp.)	63	87	80K ($\times 3.70$)	16M(2+10+4) ($\times 3.70$)	3.10ms=(0.52+1.74+0.84) ($\times 2.23$)
i4d	144	288	373K(62%)	73M(62%)	8.93ms
i4d* (imp.)	67	105	103K ($\times 3.62$)	20M(2+12+6) ($\times 3.62$)	3.67ms=(0.61+2.03+1.04) ($\times 2.43$)
i4e	160	320	461K(60%)	90M(60%)	10.90ms
i4e* (imp.)	97	131	172K ($\times 2.68$)	34M(3+22+8) ($\times 2.68$)	5.45ms=(0.76+3.35+1.34) ($\times 2.00$)
i5a	160	320	461K(44%)	23M(44%)	3.96ms
i5a* (imp.)	91	139	173K ($\times 2.67$)	8M(1+6+2) ($\times 2.67$)	2.55ms=(0.41+1.55+0.59) ($\times 1.55$)
i5b	192	384	664K(46%)	33M(46%)	5.71ms
i5b* (imp.)	108	178	262K ($\times 2.53$)	13M(1+8+3) ($\times 2.53$)	3.28ms=(0.51+1.95+0.82) ($\times 1.74$)

Table 5: Layerwis analysis on *VGG-16*. We do not compress the first convolutional layer and fully-connected layers as done in Zhang et al. (2015a). The theoretical speed-up ratio of convolutional layers and whole layers are $\times 5.03$ and $\times 4.93$ respectively. (S : input channel dimension, T : output channel dimension, (R_3, R_4) : Tucker-2 rank).

Layer	S/R_3	T/R_4	Weights	FLOPs	S6
C_{12}	64	64	37K	1853M	234.58ms
C_{12}^* (imp.)	11	18	4K ($\times 10.15$)	182M(=35+89+58) ($\times 10.15$)	64.35ms(= 13.42+28.46+20.47) ($\times 3.65$)
C_{21}	64	128	74K	926M	105.66ms
C_{21}^* (imp.)	22	34	8K ($\times 9.17$)	101M(=8+38+55) ($\times 9.17$)	23.20ms(=3.26+7.82+12.12) ($\times 4.55$)
C_{22}	128	128	148K	1851M	226.29ms
C_{22}^* (imp.)	39	36	22K ($\times 6.64$)	279(=63+159+58) ($\times 6.64$)	50.66ms(=11.60+27.19+11.86) ($\times 4.47$)
C_{31}	128	256	295K	926M	93.71ms
C_{31}^* (imp.)	58	117	74K ($\times 4.01$)	231M(=15+122+94) ($\times 4.01$)	29.92ms(=2.96+14.73+12.23) ($\times 3.13$)
C_{32}	2562	256	590K	1850M	211.75ms
C_{32}^* (imp.)	138	132	76K ($\times 7.81$)	237M(=55+129+53) ($\times 7.81$)	34.16ms(=7.94+17.89+8.33) ($\times 6.20$)
C_{33}	256	256	590K	1850M	213.31ms
C_{33}^* (imp.)	124	119	195K ($\times 3.03$)	612M(=100+416+96) ($\times 3.03$)	72.66ms(=12.74+47.74+12.19) ($\times 2.94$)
C_{41}	256	512	1180K	925M	98.40ms
C_{41}^* (imp.)	148	194	265K ($\times 4.45$)	208M(=17+114+78) ($\times 4.45$)	23.58ms(=2.54+12.25+8.79) ($\times 4.17$)
C_{42}	512	512	2360K	1850M	216.16ms
C_{42}^* (imp.)	212	207	609K ($\times 3.87$)	478M(=85+310+83) ($\times 3.87$)	51.18ms(=9.10+33.22+8.86) ($\times 4.22$)
C_{43}	512	512	2360K	1850M	216.34ms
C_{43}^* (imp.)	178	163	436K ($\times 5.42$)	342M(=71+205+65) ($\times 5.42$)	38.85ms(=8.06+23.14+7.66) ($\times 5.57$)
C_{51}	512	512	2360K	463M	57.54ms
C_{51}^* (imp.)	185	164	452K ($\times 5.22$)	89M(=19+54+16) ($\times 5.22$)	13.09ms(=2.80+7.89+2.39) ($\times 4.40$)
C_{52}	512	512	2360K	463M	76.80ms
C_{52}^* (imp.)	172	170	416K ($\times 5.67$)	82M(=16+48+17) ($\times 5.67$)	11.87ms(=2.64+6.82+2.42) ($\times 6.47$)
C_{53}	512	512	2360K	463M	67.69ms
C_{53}^* (imp.)	120	120	438K ($\times 5.38$)	86M(=17+52+17) ($\times 5.38$)	12.16ms(=2.65+7.13+2.38) ($\times 5.57$)